Controller Area Network With Flexible Data Rate (CAN FD) Eye Diagram Prediction

Junyong Park, *Member, IEEE*, Manho Lee, *Member, IEEE*, Shinyoung Park, *Member, IEEE*, Jonghoon Kim, *Senior Member, IEEE*, Joungho Kim, *Fellow, IEEE*, and DongHyun Kim, *Member, IEEE*

***Abstract*—A method for predicting the eye diagram for a controller area network with a flexible data rate (CAN FD) is proposed in this article. A CAN FD changes a data rate according to the status to overcome the limitation of latency. In other words, when data to be transmitted are accumulated, the CAN FD increases the data rate up to 5 Mb/s. The CAN FD has a bus topology consisting of multiple electronic control units, which results in a significant amount of signal reflection. Thus, the above causes the signal integrity analysis uncertain. To avoid this, this article proposes a simplified model for the CAN FD and the eye diagram prediction method based on it. The proposed method has the deterministic and statistical: the deterministic part uses an iterative single bit response method for bit probabilities of a CAN FD packet, and the statistical part uses a modified double edge response method for the flexible data rate. For verification, this article compares the predicted eye diagram to the measured eye diagram, and they are nearly the same when the CAN FD operates at the nominal data rate of 1 and optional data rate of 2 Mb/s.**

***Index Terms*—Automotive system, controller area network with flexible data rate (CAN FD), eye diagram, flexible data rate, modeling, prediction method, signal integrity (SI).**

I. Introduction

CURRENT vehicle systems include several types of electronic control units (ECUs) to control over 30 000 parts. The vehicle systems control the ECUs with various types of networks depending on their complexity and the data rate [1], [2], [3]. Most of the vehicle systems use the combined network with the local interconnect network (LIN) and the controller area network (CAN). The LIN consists of a single master and multiple slaves to communicate between ECUs [4], [5]. Since the LIN is a serial network protocol, it achieves low cost [6]. The CAN supports multiple masters and multiple slaves, which reduces wiring cost, complexity, and weight compared to multiple point-to-point wiring systems [7], [8], [9], [10]. The CAN has two characteristics: 1) priority-based communication and 2) multimaster communication. Each ECU has a priority depending on its importance. Thus, if the ECU with the highest priority sends data, other ECUs receive the data from only the bus. That is, the ECU with the lowest priority should wait until the others finish transmitting the data, which causes a latency. To overcome the latency, the CAN with flexible data rate (CAN FD) was proposed [11]. The CAN FD increases the data rate up to 5 Mb/s during the data field transmission. The increased data rate is defined as an optional data rate.

ECUs transmit and receive data on the same bus, which results in the CAN FD having critical signal integrity (SI) issues [15]. Multiple ECUs are distributed and connected in an automotive system; thus, the channel length of the CAN FD is greater than that of other high-speed systems. The number of the connected ECUs, stubs, and long channel make a significant amount of signal reflection on the CAN FD bus. Also, each ECU has different channel characteristics due to the stubs. Therefore, the SI analysis with an eye diagram is required for the CAN FD. The eye diagram is obtained by accumulating the received waveforms at the data rate of interest. As shown in Fig. 1, because the CAN FD changes the data length and data rate during the data field transmission, the eye diagram obtained in a conventional manner has rising and falling edges in the middle of the eye diagram. The signal reflection also causes the edges. The edges in the eye diagram become uncertain, which results in the limited SI analysis for the CAN FD. Therefore, a method to achieve the SI analysis on the CAN FD is required for the flexible data rate and signal reflection.

An eye diagram acquisition is time-consuming because the eye diagram is obtained by the superposition of the received waveforms. Hence, eye diagram prediction methods were proposed to obtain the eye diagram by using the channel response in an efficient manner [13], [14], [15]. The first proposed method to predict an eye diagram was based on a single bit response (SBR) [13]. The SBR method was limited when rising and falling responses were not mirrored, a double edge response (DER) based prediction method was proposed [15]. Prediction methods at the system level were also proposed [16], [17], [18], [19], [20]. The encodings to improve the channel performances [16], multilevel signaling to reduce the required bandwidth for

Manuscript received 23 September 2023; revised 17 November 2023; accepted 30 December 2023. Date of publication 17 January 2024; date of current version 13 June 2024. This work was supported by the National Science Foundation under Grant IIP-1916535 and equipment loaned by Rohde and Schwarz. *(Corresponding author: Junyong Park.)*

Junyong Park and DongHyun Kim are with the Electromagnetic Compatibility Laboratory, Missouri University of Science and Technology, Rolla, MO 65409 USA (e-mail: junyongpark@mst.edu; dkim@mst.edu).

Manho Lee is with the Samsung Electronics Company Ltd., Hwaseong 445-3330, South Korea (e-mail: leemanho@me.com).

Shinyoung Park is with the Rambus, San Jose, CA 95134 USA (e-mail: parks@rambus.com).

Jonghoon Kim and Joungho Kim are with the Terabyte Interconnection and Package Laboratory, Korea Advanced Institute of Science and Technology, Daejeon 305-701, South Korea (e-mail: jonghoon@kaist.ac.kr; joungho@kaist.ac.kr).

Color versions of one or more figures in this article are available at https://doi.org/10.1109/TEMC.2024.3350054.

Digital Object Identifier 10.1109/TEMC.2024.3350054

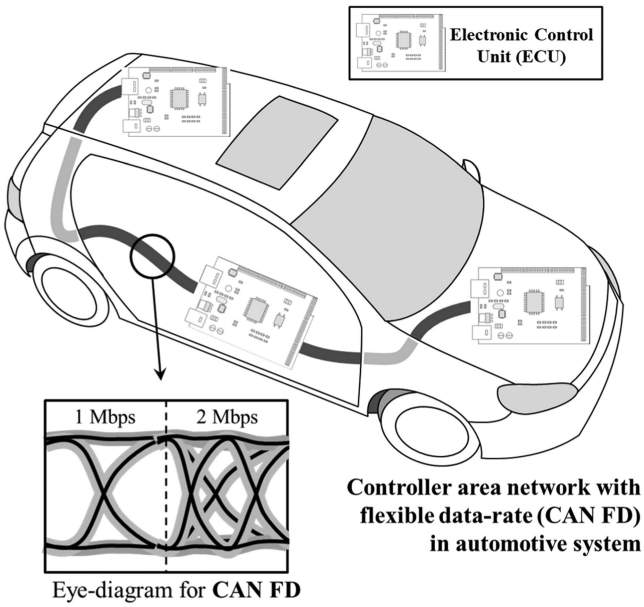

Fig. 1. CAN FD in an automotive system. Because the CAN FD can change a data rate in the middle of transmission, the corresponding eye diagram may be misinterpreted.

the channel [17], pseudorandom bit sequences to SI analysis [18], and error correction code to correct bit errors [19] were considered in the statistical eye diagram at the system level. The proposed methods were under the assumption that the data is transmitted and received at the data rate of the fixed value. Also, the CAN FD transmits the data in the form of a packet. Thus, it includes deterministic parts in the data. The proposed prediction method covers not only the flexible data rate but also the deterministic part of the packet for reliable signal integrity analysis for the CAN FD. In this article, the nominal data rate is 1 Mb/s and the optional data rate is 2 Mb/s for the data field transmission. The optional data rate is available up to 5 Mb/s, however, the measurement setup has signal reflections. Thus, the optional data rate is limited to 2 Mb/s in the measurement setup.

The rest of this article is organized as follows. In Section II, we introduce the overall algorithm and demonstrate why the proposed method provides accurate results. Section III describes the bit probability density function (pdf) model for a CAN FD packet. The probability model is obtained from how the CAN FD works. We apply the method proposed herein to the CAN FD channel. The channel response, as the input of the proposed method, is obtained from the simplified model for the CAN FD in SPICE. Section IV proposes an eye diagram prediction method based on the simplified CAN FD channel. Section V proposes application to the CAN FD. Finally, Section VI concludes this article.

II. Proposed Prediction Method for the CAN FD

This section demonstrates the overall algorithm of the proposed method; this section also covers why the proposed method consists of the SBR-based [13] and DER-based [15] methods. The SBR method is for deterministic bit probabilities, and the DER method is for a flexible data rate. The SBR method is based on a SBR, thus, the flexible data rate cannot be dealt with. The DER method is not applicable to the deterministic bit probabilities, because the probabilities for the rising and falling edges are only considered. The CAN FD packet includes a flexible data rate and a deterministic bit PDF as well. Therefore, the SBR and DER methods should be combined to evaluate the statistical eye diagram for the CAN FD.

A. Overall Algorithm of the Proposed Method

Fig. 2 shows the overall algorithm of the proposed method. The proposed method consists of the iterative SBR method and modified DER method for the arbitration and data phase, respectively. The iterative SBR has an iterative loop with bit probability distribution that arbitration process defined by the CAN FD specification is expressed with respect to probability. The modified DER has an additional delay block to generate the response for the flexible data rate. A simplified equivalent CAN FD model generates the channel response. The equivalent model consists of a simplified ECU model and twisted pair cables to represent the CAN FD bus. Thus, the channel responses generated by the equivalent model are applied to the iterative SBR and modified DER methods, respectively.

The first and second arbitration phases have a fixed data rate, but their bit probabilities depend on the bit location in a CAN FD packet. Thus, the statistical eye diagram is obtained from the iterative SBR method to consider the effect depending on the bit location. The SBR is divided into main cursor and inter-symbol interference (ISI) pdf to obtain the total pdf. Because the probability of ONEs and ZEROs also affects the total pdf, the bit probability distribution depending on the bit location $P(X_i) = 1$ is also introduced herein. The number of iterations is equal to the length of the first and second arbitration phases, respectively. Then, the weighted summation is applied to the obtained statistical eye diagrams for the arbitration phase.

The statistical eye diagrams for the flexible data rate are obtained by the modified DER method. The modified DER method is the DER method with a delay Δt to either rising or falling response for a flexible data rate. In the CAN FD, the data rate is determined by the priority of the ECU and the channel status. Therefore, for generalization, the weighting factors for the data rate are introduced.

After obtaining the statistical eye diagrams for the arbitration phase and data phase, the statistical eye diagram for the CAN FD is obtained by the weighted summation. The weighting factor is determined by how much they occupy the CAN FD packet. The length of each phase varies depending on the channel status; thus, the weighting factor is also introduced to generalize the algorithm.

B. Comparison Between the SBR- and DER-Based Method

The principle of the SBR-based method [13] is the same as that of the DER-based method [15], as follows. First, the ISI pdf in an amplitude domain for a digital state of ZERO is obtained. The pdf in the amplitude domain for a digital state of ONE is

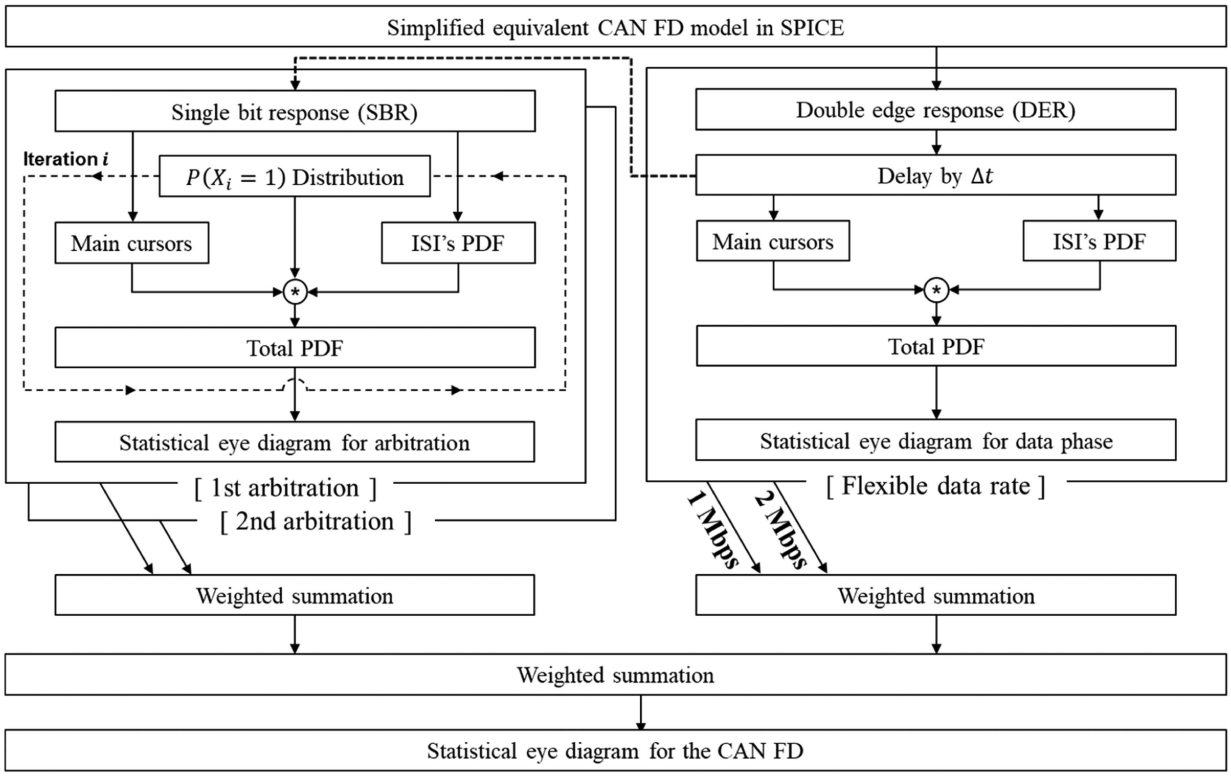

Fig. 2. Overall algorithm for the proposed method for the CAN FD. The proposed method consists of the iterative SBR method and modified DER method.

obtained by a convolution of a main cursor and the ISI pdf for the same sampling time. The main difference between the SBR and DER is an input for each algorithm, as shown in Fig. 3, which leads to different algorithms and results. The SBR and DER methods have the same assumption that a channel is a linear and time-invariant system. However, the SBR assumes the rising and falling responses are symmetric, which means that pull-up and -down are mirrored. The DER has inputs of rising and falling responses because it assumes that the rising and falling responses are asymmetric. By having the rising and falling response as the input, the DER can deal with the controllable data rate, as shown in Fig. 3(b). If a smaller amount of delay between the rising and falling responses is applied, then it would be the single bit response for a higher data rate. Thus, the channel response can be obtained for any data rate if the rising and falling responses are given. The above characteristic of the DER method makes the proposed method generalized for any data rate and the number of optional data rates. The practical CAN FD bus may have an overshoot or undershoot on the rising and falling response. Since the SBR was generated from the delayed DER, degradations on rising and falling responses are reflected.

The CAN FD supports two data rates: 1) a standard rate of 1 Mb/s and 2) an optional rate of 2 Mb/s. The characteristic of a higher data rate only applies to a portion of the data packet, and the other portion is transmitted at the standard data rate. In other words, the data packet is divided into two groups: flexible and fixed groups in terms of the data rate. The fixed group is related to the CAN FD protocol. The protocol defines a rule for how the data is transmitted and received between ECUs,

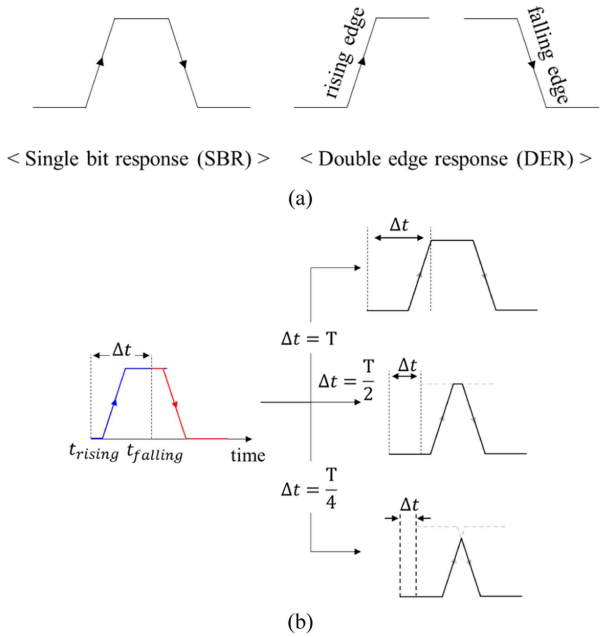

Fig. 3. (a) Eye diagram can be predicted according to two types of channel responses: SBR and DER. (b) In case of the DER, the data rate of the eye diagram is controllable according to the time difference between the rising and falling response.

which results in the fixed group can be expressed in the form of probability. Table I shows the above that compares the SBR and DER methods with respect to the input, data rate, and bit PDF.

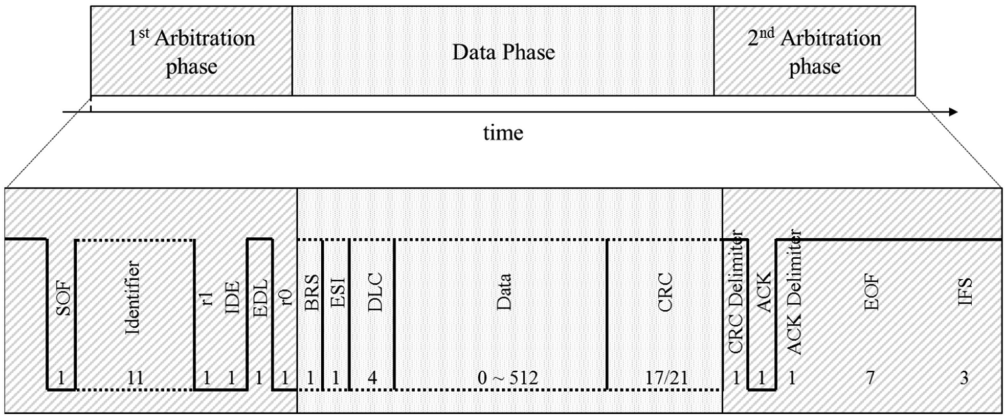

Fig. 4. CAN FD packet consisting of an arbitration phase and a data phase. The CAN FD provides a flexible data rate option for the data phase.

TABLE I
COMPARISON OF THE SBR-BASED AND DER-BASED METHODS

Method	Details
SBR	**Input**: Channel response by single bit Single bit: 0001000000… **Data rate**: Fixed single value Bit PDF, $P(X_i = 1)$, for **convolution**
DER	**Input**: Channel responses by bit transition (rise and fall) Rise: 00001111111… Fall: 11110000000… **Data rate**: Controllable value by UI Bit transition PDF, $P(X_iX_{i-1} = 10\ or\ 01)$, for **convolution**

III. BIT PDF OF THE CAN FD PACKET

In this section, we obtain the bit pdf from the CAN FD packet. The SBR-based method estimates the eye diagram with the bit pdf obtained in this section.

A. Introduction to the CAN FD Packet

The CAN FD uses packet-based communication. Fig. 4 shows how a CAN FD packet consists of the first, second arbitration, and data phases. The purpose of the first arbitration phase is to negotiate among ECUs and notify them of the data transmission and condition. The first arbitration phase includes the start of the frame (SOF), the identifier, the identifier extension (IDE), and the extended data length (EDL). The SOF provides notification of the start of the packet, and the identifier indicates the priority of the ECU. The ECU with a higher value of identifier has a higher priority on the CAN FD bus. The second arbitration phase is responsible for termination notification to other ECUs. The second arbitration phase includes acknowledge (ACK), end of frame (EOF), and interframe space (IFS). As mentioned above, the standard data rate of the CAN FD is 1 Mb/s [14]. The first and second arbitration phases are transmitted at the data rate of 1 Mb/s.

The data phase contains the control field, data field, and error-detection field. The control field shows the data transmission condition, whereas the error-detection field improves the data reliability with redundant data. The control field represents the data length in bytes and its data rate. The control field has the bit rate switch (BRS), error state indicator (ESI), and data length code (DLC). If the BRS field is ONE, then the data rate would be up to 8 Mb/s; if not, the data rate would be the same as that in the other phases. The other bits in the data field and the other fields are transmitted at the standard data rate of 1 Mb/s. The DLC bits represent the length of the data field. If the most significant bit (MSB) is ZERO, the following three bits indicate the data length in bytes. If the MSB is ONE, the data length in bytes is determined by a look-up table, in which the data length is defined as 8, 12, 16, 20, 24, 32, 48, or 64 bytes. The error-detection field is the cyclic redundant code (CRC) to detect errors in the data field. The bit length of the CRC is 17 if the length of the data is smaller than 20 bytes, otherwise 21.

B. Bit PDF of the First and Second Arbitration Phases

The SOF field is always ZERO, thus, the probability for ZERO is equal to 1. The next field is the identifier that represents the priority of each ECU. At this stage, the waiting ECUs transmit their identifiers on the CAN FD bus simultaneously. As a result, the ECU with the highest priority transmits the identifier and the other ECUs would halt the identifier transmission. In the binary system, the shift left by 1 bit is equivalent to multiplication by 2. Thus, a greater number has ONE on the further left bit location. All ECUs transmits the identifier field and the ECUs with smaller identifier value halt when they detect higher identifier value. The resultant identifier field has a lower ONE's probability at the further right bit index. The most left ONE shows a higher identifier and other ONEs are insignificant in terms of priority. Therefore, the ONE's probability becomes lower as the bit index increases

$$P\left(X_i = 1\right) = 1 - \left(2^{N-i+2}\right)^{-1} \tag{1}$$

where N is the number of the connected ECUs on the CAN FD bus and i is the bit position. The remaining bits of the first

TABLE II
$P(X_i{=}1)$ DISTRIBUTION IN THE FIRST ARBITRATION PHASE

i	1	2	3	4	5	6	7	8
P	1	$1-(2^{N-i+2})^{-1}$						
i	9	10	11	12	13	14	15	16
P	$1-(2^{N-i+2})^{-1}$				1	1	0	1

TABLE III
$P(X_i{=}1)$ DISTRIBUTION IN THE SECOND ARBITRATION PHASE

i	1	2	3	4	5	6	7	8
P	0	1	0	0	0	0	0	0
i	9	10	11	12	13			
P	0	0	0	0	0			

arbitration phase are r1, IDE, EDL, and r0. Their bits are always fixed at "11 01," and they are deterministic. Table II shows the 1's probability distribution depending on the bit index for the first arbitration field. The bits marked as white represent the deterministic; the bits marked as gray represent statistical.

The second arbitration phase has a simpler bit pdf than the first arbitration phase. The bits in the second phase are fixed at "01 00 00 00 00 00 0". Thus, the second arbitration field is deterministic, as shown in Table III.

C. Bit PDF of the Data Phase in the CAN FD Packet

The data phase consists of the control field, data field, and error-detection field. We assume that no information is given for the data field, and thus, every bit in the data field has a uniform bit pdf. As discussed earlier, the DLC represents the length of the data field. The available data field lengths are 0, 1, 2, 3, 4, 5, 6, 7, 8, 12, 16, 20, 24, 32, 48, and 64 bytes. If the above assumption is applied to the DLC bits, the length will be one of the lists with a probability of 1/16 for each length. The remaining bits of the data phase detect whether errors occur in the data field. In this case, since the divider is not given, we assume that the CRC bits are uniformly distributed probabilities for ONE and ZERO because the CRC bits are considered purely random bits. The CRC bits are the results of the redundancy calculation. Therefore, we assumed that the CRC bits are uniformly distributed probabilities for ONEs and ZEROs.

IV. EYE DIAGRAM PREDICTION FOR THE CAN FD

This section includes details on statistical eye diagram prediction with the bit pdfs obtained from the previous section. The SBR method is for the first, the second arbitration phase, and a portion of the data phase at the standard data rate. The DER method is for the data field in the data phase.

A. Weighting Factor for Flexible Data Length in the CAN FD

The CAN FD accommodates not only a flexible data rate but also a flexible data length. Because the data phase has various data lengths depending on the DLC bits, this characteristic affects the eye diagram. To predict an accurate eye diagram, we introduce a weighting factor representing the ratio of the corresponding phase in the CAN FD eye diagram. Each bit of the CAN FD equally contributes to the eye diagram; thus, the most dominant phase has the largest weighting factor. The meaning of the most dominant phase is that the phase has the longest data length among other phases. To analyze the CAN FD packet with respect to the data length and determine the weighting factor, Table IV shows the number of bits in the CAN FD packet. The first arbitration phase, data phase, and second arbitration phase have 16, 23–539, and 13 bits, respectively. Let L_{data} denote the length of the data phase, and then the weighting factors for the first and second arbitration phase are followings as:

TABLE IV
NUMBER OF BITS IN A CAN FD PACKET

Phase	Field	Number of bits	
1st arbitration	SOF	1	16
	Identifier	11	
	r1	1	
	IDE	1	
	EDL	1	
	r0	1	
Data	BRS	1	23-539
	ESI	1	
	DLC	4	
	Data	0–512	
	CRC	17 or 21	
2nd arbitration	CRC delimiter	1	13
	ACK	1	
	ACK delimiter	1	
	EOF	7	
	IFS	3	

$$w_{arb1} = \frac{16}{16 + L_{\text{data}} + 13} \tag{2}$$

$$w_{arb2} = \frac{13}{16 + L_{\text{data}} + 13}. \tag{3}$$

Therefore, the eye diagram for the CAN FD $\text{Eye}_{\text{CAN FD}}$ is produced according to

$$\text{eye}_{\text{CAN FD}} = w_{arb1} \cdot \text{eye}_{arb1} + w_{data} \cdot \text{eye}_{\text{data}} + w_{arb2} \cdot \text{eye}_{arb2} \tag{4}$$

where w_{data} is the weighting factor for the eye diagram by the data phase, w_{arb1} is the weighting factor for the eye diagram by the first arbitration field, and w_{arb2} is the second arbitration field.

B. Weighting Factor for the Flexible Data Rate in the CAN FD

The BRS bit in the data phase indicates whether the data rate of the data field is the optional or the standard value. That is, the data rate of the data phase is 1 or 2 Mb/s, depending on the BRS bit, because the optional data rate is 2 Mb/s herein. As shown in

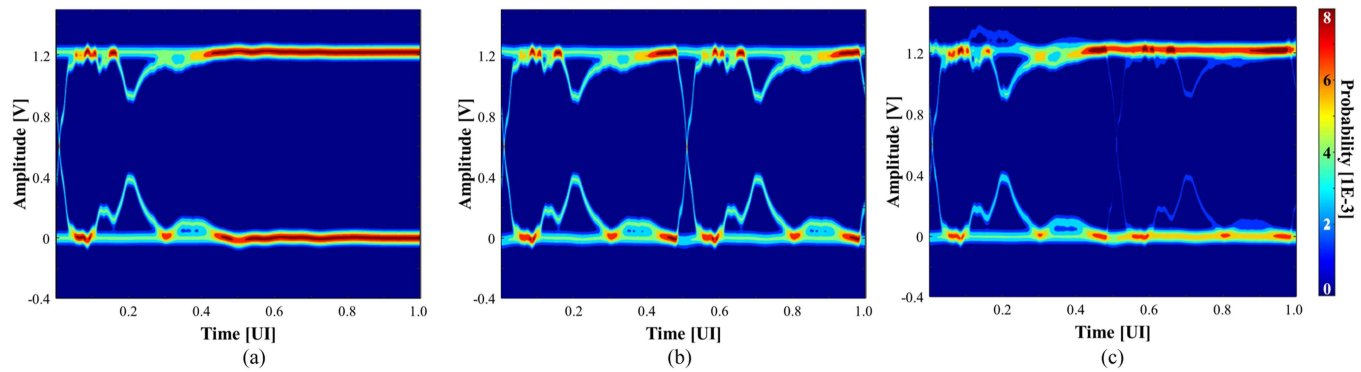

Fig. 5. Statistical eye-diagram for the data phase at the date-rate of (a) 1 Mb/s ($\text{eye}_{1\text{Mb/s}}$) and (b) 2 Mb/s ($\text{eye}_{2\text{Mb/s}}$). (c) Statistical eye-diagram for the data phase is obtained by summing the statistical eye-diagrams (eye_{DATA}) at data rates of 1 and 2 Mb/s.

Fig. 5(a) and (b), the modified DER method generates statistical eye diagrams at 1 Mb/s ($\text{eye}_{1\text{Mb/s}}$) and 2 Mb/s ($\text{eye}_{2\text{Mb/s}}$). After the statistical eye diagrams are obtained at data rates of 1 and 2 Mb/s, the eye diagram for the flexible data rate is obtained by weighted summation of the statistical eye diagrams for 1 and 2 Mb/s. Fig. 5(c) shows the result of the above procedure, which has the rising and falling edges in the middle. The edges in the middle can be thought of as reflections from other ECUs on the CAN FD bus. In the fixed data rate, the edges in the middle of the eye diagram typically occur by signal reflection or crosstalk. The advantage of the merged eye diagram is to make the edges in the middle distinguishable from flexible data rate, signal reflection, and crosstalk. Therefore, the proposed method achieves the separation of the flexible data rate from the other degradations.

The probability of the BRS bit P_{BRS} determines, which data rate is dominant in the data field. The statistical eye diagram for the flexible data rate is obtained as follows. The eye diagram at 2 Mb/s is weighted by P_{BRS}, whereas the eye diagram at 1 Mb/s is weighted by the complement of the BRS probability $P^{C}{}_{\text{BRS}}$

$$\text{eye}_{\text{FLEX}} = P_{\text{BRS}} \cdot \text{eye}_{2\text{Mb/s}} + P^{C}_{\text{BRS}} \cdot \text{eye}_{1\text{Mb/s}}. \quad (5)$$

The probability of the bit rate switch P_{BRS} is related to the priority of the ECU. It is also affected by how many packets are accumulated before transmission. Therefore, the probability of the bit rate switch is a variable that can be always controlled depending on the channel status and the priority of the ECU of interest.

C. Statistical Eye Diagram for the Data Phase

Fig. 6 shows the overall algorithm used to predict the eye diagram for the data phase. The obtained eye diagram for the flexible data rate is weighted by the ratio of the flexible data length and summed, as described in

$$\text{eye}_{\text{DATA}} = \text{eye}_{\text{FLEX}} \cdot \frac{L_{\text{flex}}}{L_{\text{data}}} + \text{eye}_{1\text{Mb/s}} \cdot \frac{(L_{\text{data}} - L_{\text{flex}})}{L_{\text{data}}} \quad (6)$$

where L_{flex} denote the length of the flexible data in the data phase, and L_{data} denote the length of the data phase. Therefore, the statistical eye diagram for the data phase is the result from the weighted summation of the eye diagrams for the flexible and nonflexible portions; the eye diagram for the flexible portion is obtained by the weighted summation of the eye diagrams for the 1 and 2 Mb/s.

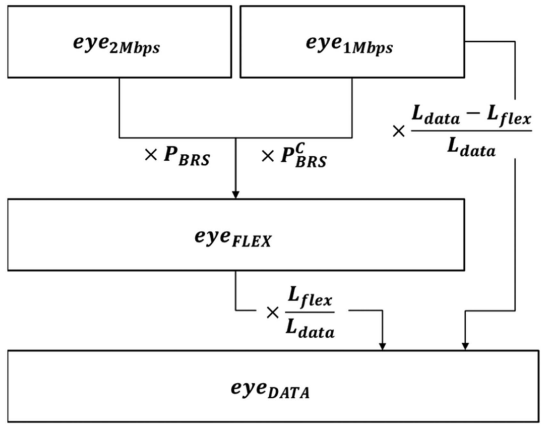

Fig. 6. Procedure to predict the eye-diagram for the data phase.

TABLE V
COMPARISON BETWEEN THE PROPOSED METHOD AND MEASUREMENT

Item	Method	Value
Eye height (EH)	Proposed method	0.238 V
	Measurement	0.205 V
Eye width (EW)	Proposed method	0.243 UI
	Measurement	0.240 UI

D. Statistical Eye Diagram for the Arbitration Phases

The iterative SBR method provides the bit location-dependent statistical eye diagram at the standard data rate. The obtained $P(X_i = 1)$ distribution in the previous section is used in this procedure. The received waveform $y(t)$ is expressed as follows:

$$y(t) = \sum_{i=-\infty}^{\infty} y_i(t), \ 0 \le t \le 1\,UI \quad (7)$$

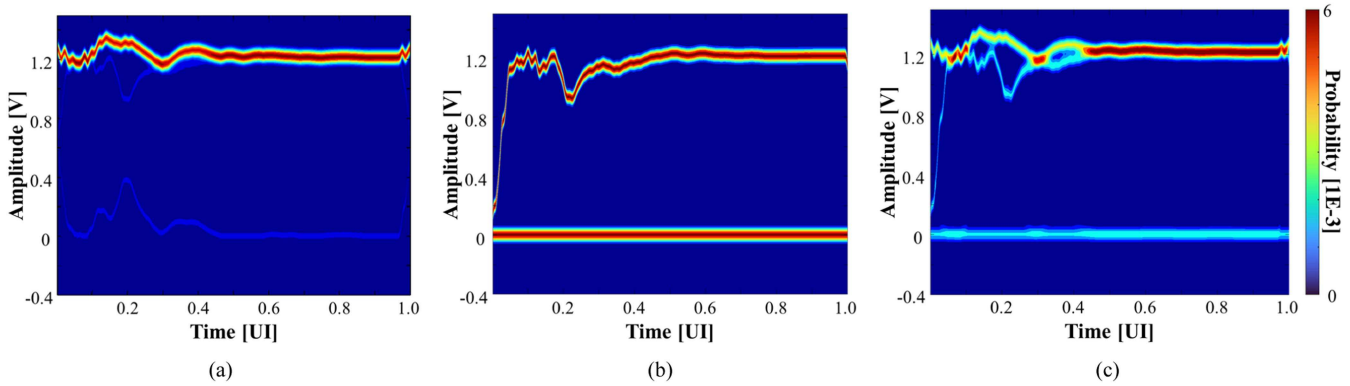

Fig. 7. Statistical eye-diagram for (a) the first arbitration phase (eye$_{arb1}$) and (b) the second arbitration phase (eye$_{arb2}$). (c) Statistical eye-diagram for the arbitration phase is obtained by summing the statistical eye-diagram for the weighted first and second arbitration phases.

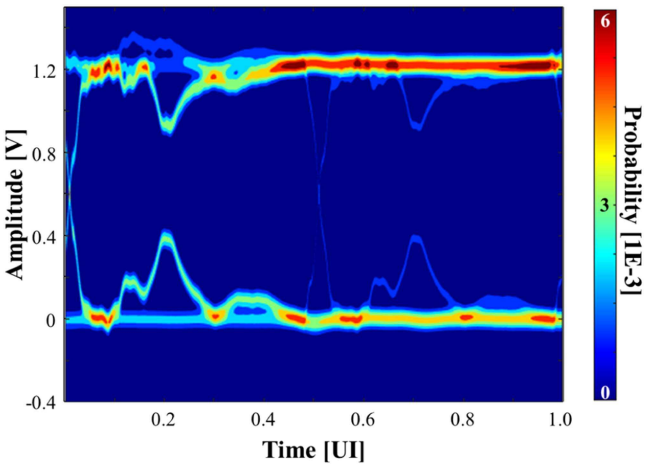

Fig. 8. Statistical eye-diagram for the CAN FD packet when single ECU transmits the packet.

$$y_{N-1}\ (t-1UI) = y_N\ (t) = y_{N+1}\ (t+1UI) \tag{8}$$

where *N* is an integer and *UI* is a bit duration time. Equation (7) shows the received waveform can be expressed as the summation of the subdivided waveforms. Each subdivided waveform $y_i(t)$ has nonzero values in a range of 0 to 1 UI in the time domain. Equation (8) shows further the definition of the subdivided waveform, and the subscripts *N-1*, *N*, and *N+1* represent subdivision indices. Then, the received waveform is divided into the main, pre-, and postcursors depending on the sampling time

$$y\ (t) = \begin{cases} y_{-N}\,(t)\,,\ t \le t_X \\ y_0\,(t)\,,\ t_X < t \le t_X + 1\,UI \\ y_N\,(t)\,,\ t > t_X + 1\,UI \end{cases} \tag{9}$$

where t_X is a starting time of the statistical eye diagram. Let $g_N(\alpha, t_S, i)$ denote the amplitude α pdf when the sampling time t_S and the main cursor is at the location of *i*

$$\begin{aligned} g_N\ (\alpha, t_S, i) &= \mathrm{P}\,(X_i = 0)\ \cdot \delta\,(\alpha) \\ &\quad + \mathrm{P}\,(\,X_i = 1) \cdot \delta\,(a - y_N\,(t_S)) \end{aligned} \tag{10}$$

where *N, i* are integers. The sampling time t_S is in a range of 0 to 1 UI and location index *i* has a range of 1 to phase length. Then, the amplitude pdf of the ISI noise is obtained by consecutive convolutions as follows:

$$\begin{aligned} &g_{\pm}\ (\alpha, t_S, i) = g_{+}\ (\alpha, t_S, i) \circledast g_{-}\,(\alpha, t_S, i)\,, \\ &\text{where}\ \ g_{+}\ (\alpha, t_s, i) = \circledast_{N=1}^{\infty}\, g_N\,(\alpha, t_S, i) \\ &g_{-}\ (\alpha, t_s, i) = \circledast_{N=-\infty}^{-1}\, g_N\,(\alpha, t_S, i)\,. \end{aligned} \tag{11}$$

The convolutions are applied when the parameter N is 1 to infinity for positive ISI and negative infinity to -1 for negative ISI. Since the single bit response depends on the data rate, the equation includes infinity to represent. The amplitude pdf at the sampling time t_S is obtained by the summation, as shown in

$$g\ (\alpha, t_S, i) = g_{\pm}\ (\alpha, t_S, i) + g_{\pm}\,(\alpha - y_0\,(t_S)\,, t_S, i)\,. \tag{12}$$

The statistical eye diagram when the main cursor is at the location of i is defined as

$$\mathrm{eye}_i = \bigcup_{t_S=0}^{1\ UI} \bigcup_{\alpha=y_{\min}}^{y_{\max}} g\,(\alpha, t_S,\ i)\,. \tag{13}$$

The variable *i* in the $P(\ X_i = 1)$ refers to the location of the main cursor in the SBR method. In the case of the first arbitration phase, if the variable i is equal to 4, the following postcursors would have ONE's probabilities from the $P(\ X_i = 1)$ distribution for $i = 5, 6, 7, \ldots$ Likewise, the precursors have ONE's probabilities from the $P(\ X_i = 1)$ distribution when $i = 3, 2, 1, 16, 15, \ldots$ Therefore, the number of the obtained statistical eye diagrams by the iterative SBR method is equal to the length of the $P(\ X_i = 1)$ distribution. Each bit has the same probability of being the main cursor, in other words, their pdf is a uniform distribution. Let $\mathrm{L_{pdf}}$ denote the length of the $P(\ X_i = 1)$ distribution, then the statistical eye diagrams for the first arbitration are given by the following:

$$\mathrm{eye}_{arb1} = \frac{1}{L_{\mathrm{pdf}}} \sum_{i=1}^{L_{\mathrm{pdf}}} \mathrm{eye}_i. \tag{14}$$

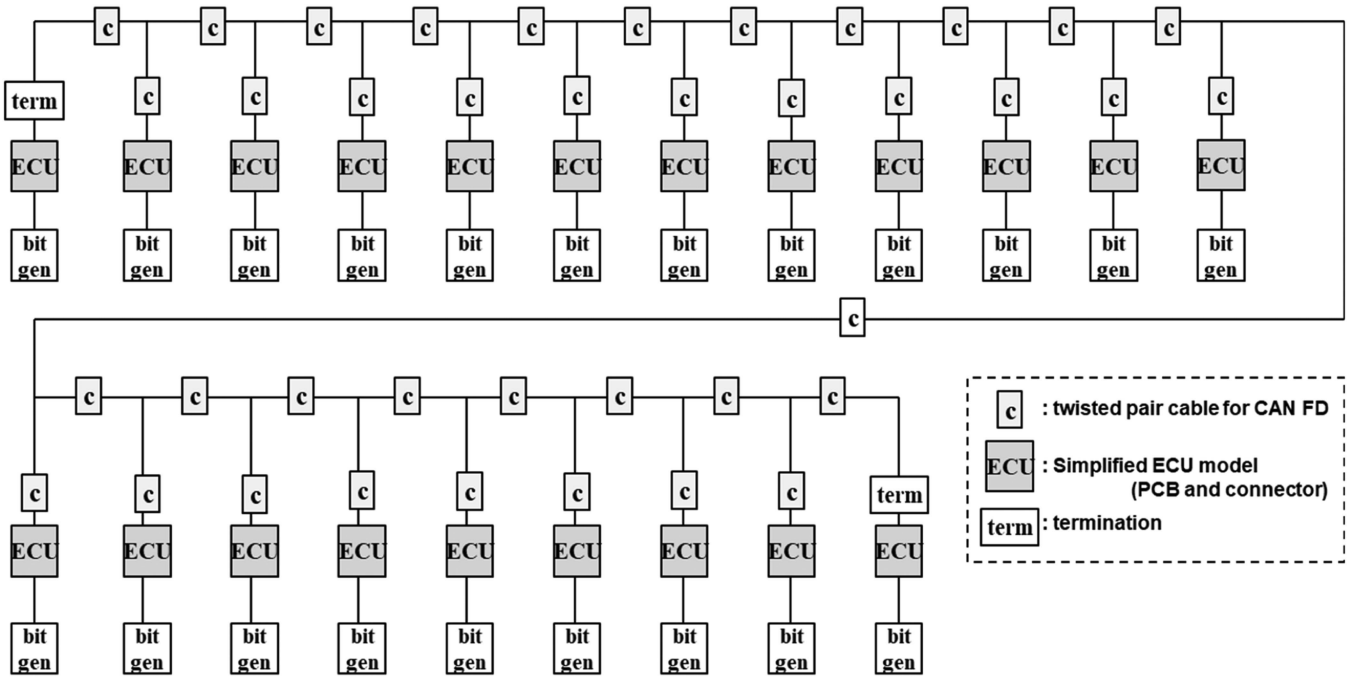

Fig. 9. Simplified CAN FD bus in SPICE. The simplified model includes multiple simplified ECU models, and they are connected by twisted pair cables.

The above procedure is also applied to the second arbitration phases with the introduced $P(X_i = 1)$ distribution, and a portion of the data phase. As indicated in Fig. 7(a) and (b), the statistical eye diagrams for the first and second arbitration phases are obtained with the introduced equations. In conclusion, Fig. 7(c) shows the result obtained by the weighted summation of the Fig. 7(a) and (b). Because their probabilities are always the same which is equal to 0.5, the statistical eye diagrams are just summed up. In case the first and second arbitration phases have different probabilities, then the results would have different characteristics depending on their probabilities.

E. Statistical Eye Diagram for the CAN FD

In the previous sections, the statistical eye diagrams for the flexible and fixed data rates are obtained, respectively. The statistical eye diagram for the CAN FD would be obtained after a weighted summation of them, as shown in Fig. 8. The statistical eye diagram is calculated at the standard data rate that is equal to 1 Mb/s. The characteristic of the flexible data rate generates the rising and falling edges at the sampling time of 0.5 UI in the eye diagram. The arbitration phases cause the fluctuation at the sampling time of 0.2 UI. The result is obtained under the condition that a single master and single slave are on the CAN FD bus. Therefore, the given channel condition has no reflections on the channel.

V. Application to the CAN FD

In this section, we apply the proposed method to a practical CAN FD bus consisting of multiple ECUs. To obtain the channel response from the complex bus topology, this article proposes a simplified model for a CAN FD in SPICE.

A. Simulation Set Up for the CAN FD Bus

Since the CAN FD network has a fly-by topology, substantial signal reflection occurs during packet transmission. Also, electrical performance evaluation is nearly impossible, because of the other ECUs. Therefore, we obtain the channel responses from the simplified model for the CAN FD in SPICE. The simplified model for each ECU included a printed circuit board (PCB), package, and ideal switch. The twisted pair cable models with variable lengths provided a connection between ECUs. Fig. 9 shows the test bench including the above simplified CAN FD bus consisting of the twisted pair cables and 20 simplified ECU models. The simplified ECU model consisted of CAN FD IC and PCB, as can be seen in Fig. 10. The ECU's simplified integrated circuit model includes simple switches by metal oxide semiconductor (MOS) and the simplified PCB model consists of parasitic resistance and capacitance. The number of point-to-point packet transmissions is 380; each point-to-point communication has rising and falling edges, and single bit responses. Therefore, the total number of channel responses would be 1140. Because the acquisition time for each response was approximately 20 min, the expected total acquisition time was 380 h.

To avoid inefficiency, we considered only 10 of 380 pairs by referring the priority. The considered pairs for the transmitting and receiving ECUs were (2/4), (2/11), (2/20), (9/1), (9/8), (9/16), (9/20), (19/2), (19/17), and (19/20). We obtained the rising and falling edges, and single bit responses for the above pairs from SPICE. Since the probability that the other ECUs with lower priority transmit the data during the eye diagram acquisition is close to 0. In other words, this article only considered the effective ECUs to achieve efficient signal integrity analysis for the CAN FD bus.

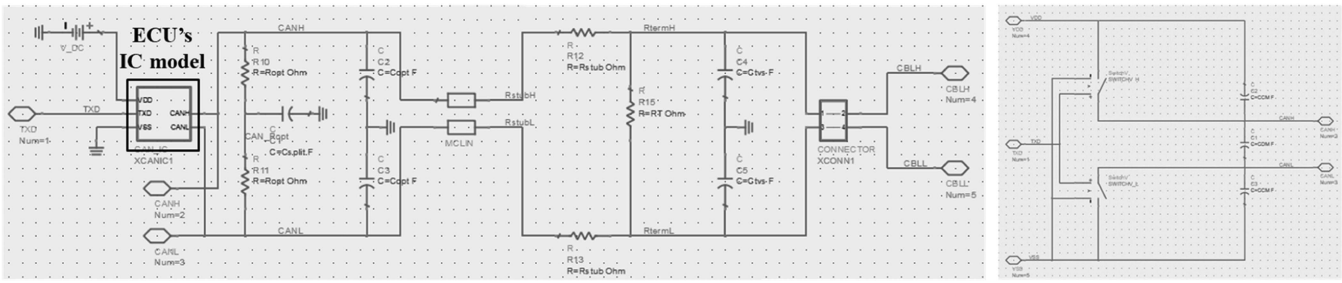

Fig. 10. Simplified ECU model consisting of (a) PCB and (b) integrated circuit (IC) in SPICE. The IC model has two ideal switches representing N/PMOS and parasitic capacitances. The PCB and connector model consist of parasitic resistance and capacitance representing the PCB and connectors on the CAN FD bus.

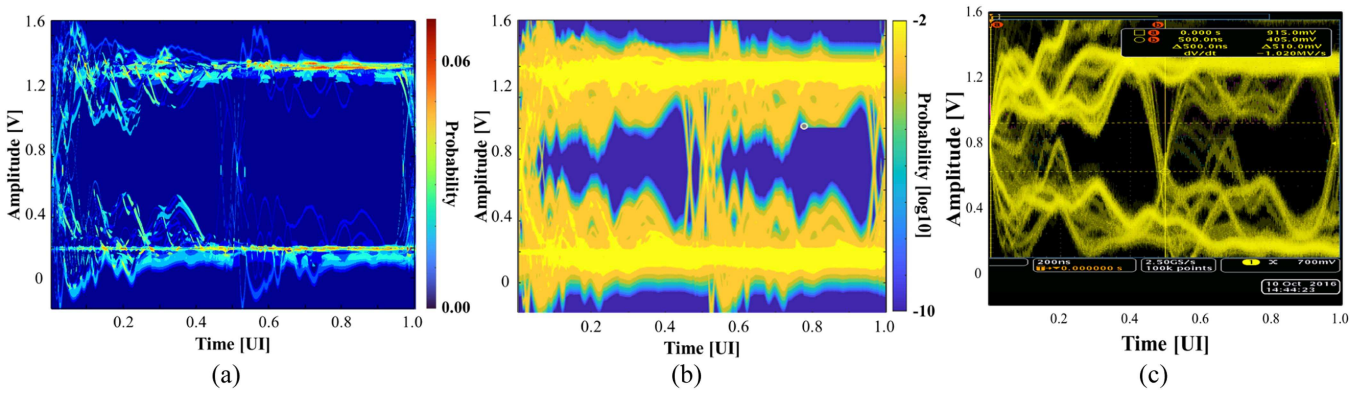

Fig. 11. Comparison of the predicted eye diagram in (a) linear and (b) log scale, and (c) the measured eye diagram. From the statistical eye diagram in the linear scale, the first edge has higher probability than that of the middle edge. The inner contour of the eye diagram was identified from the statistical eye diagram in the log scale.

B. Eye Diagram Comparison Between the Proposed Method and Measurement Results

To verify the proposed method, we measured and compared the eye diagram from the CAN FD bus. The waveforms were captured between ECU #10 and #11, and the acquisition time was approximately 10 s. The eye diagram was acquired when 20 ECUs were connected to the CAN FD bus. In the measurement setup, the priorities of the ECUs were not specified. Furthermore, the CAN FD bus consisted of twisted pair cables between ECUs, thus resulting in substantial signal reflection from other ECUs. Fig. 11 shows the predicted and measured eye diagrams for the CAN FD bus at the standard and optional data rates. We identified that the first edges of the eye diagram had a higher probability than that of the middle edges in the linear-scaled eye diagram. The log-scaled eye diagram provided the inner contour of the eye diagram, which enables system integrity validation. Although the limitations make the comparison uncertain, their profiles appear to be nearly identical. The color in each case means a probability. Both have significant fluctuations at the sampling time of 0.2 UI due to the arbitration phase, as we discussed in the previous section. Also, the signal reflections affected the fluctuation. At the sampling time of 0.5 UI, the rising and falling edges were captured due to the flexible data rate. Table V shows the eye height (EH) and eye width (EW) values for the proposed method and the measurement, respectively.

Another degrading factor for the eye diagram was a jitter depending on the ECU. The ECUs were distributed at various distances, thus resulting in variations in the propagation time. This variation also made the transition in the middle of the eye diagram shifted back and forth. Therefore, the obtained CAN FD eye diagram had two small eye diagrams from 0 to 1 UI. The measured EH and EW values were evaluated from the left eye diagram.

VI. Conclusion

The CAN FD was proposed to overcome the limitations of the CAN in automotive systems. The CAN FD improved the electrical performance, however, the characteristic of the flexible data rate caused signal integrity uncertain. That is, analysis of the CAN FD's eye diagram was hindered by the complex topology, flexible data length, and data rate in the CAN FD. To address this challenge, we proposed an eye diagram prediction method based on a simplified model for the CAN FD bus. The simplified model generated the channel responses from the CAN FD bus, and the proposed prediction method generated the statistical eye diagram based on it. The proposed method includes the iterative SBR and modified DER methods to include the effects of the CAN-FD packet on the statistical eye diagram. We measured the eye diagram for the CAN FD bus and compared it with the predicted result in the time domain.

From the comparison, their eye diagrams had similar trends and their EH and EW values were also comparable. With the proposed method and the simplified model, this article proposes a method for predicting eye diagrams for a CAN FD and demonstrates, which parameters in the CAN FD packet degrade the eye diagram.

REFERENCES

[1] S. Tuohy, M. Glavin, C. Hughes, E. Jones, M. Trivedi, and L. Kilmartin, "Intra-vehicle networks: A review," *IEEE Trans. Intell. Transp. Syst.*, vol. 16, no. 2, pp. 534–545, Apr. 2015.

[2] N. Navet and F. Simonot-Lion, "In-vehicle communication networks—A historical perspective and review," in *Industrial Communication Technology Handbook*, vol. 96, 2nd ed. Boca Raton, FL, USA: CRC Press, 2013.

[3] W. Zeng, M. A. S. Khalid, and S. Chowdhury, "In-vehicle networks outlook: Achievements and challenges," *IEEE Commun. Surv. Tut.*, vol. 18, no. 3, pp. 1552–1571, Jul.–Aug. 2016.

[4] Yumpu.com. (n.d.). Lin_specification_package_2.2a. yumpu.com. [Online]. Available: https://www.yumpu.com/en/document/read/48401977/lin-specification-package-22a

[5] M. Popa, V. Groza, and A. Botas, "Lin bus testing software," in *Proc. Can. Conf. Elect. Comput. Eng.*, 2006, pp. 1287–1290, doi: 10.1109/CCECE.2006.277634.

[6] Interfacebus.com, "LIN bus description, automotive bus, local interconnect network," 2015. Accessed: Aug. 15, 2018. [Online]. Available: http://www.interfacebus.com/Design_Connector_LIN_Bus.html

[7] Can in automation (CIA), "CAN in Automation (CiA): History of the CAN technology." Accessed: Jan. 10, 2024. [Online]. Available: https://www.can-cia.org/can-knowledge/can/can-history/

[8] ISO 11898-2:2016. ISO, May 27, 2022.

[9] Bosch - University of California, Riverside. (n.d.). [Online]. Available: http://esd.cs.ucr.edu/webres/can20.pdf

[10] M. Di Natale et al., *Understanding and Using the Controller Area Network Communication Protocol*. Berlin, Germany: Springer, 2012.

[11] Can in automation (CIA), "CAN in automation (CiA): CAN FD - the basic idea." Accessed: Jan. 10, 2024. [Online]. Available: https://www.can-cia.org/can-knowledge/can/can-fd/

[12] S. Park et al., "Signal integrity analysis of automotive CAN-FD networks with series damping resistor-equipped joint connectors," in *Proc. IEEE Elect. Des. Adv. Packag. Syst.*, 2020, pp. 1–3, doi: 10.1109/EDAPS50281.2020.9312922.

[13] B. K. Casper, M. Haycock, and R. Mooney, "An accurate and efficient analysis method for multi-gb/s chip-to-chip signaling schemes," in *Proc. Symp. VLSI Circuits. Dig. Tech. Papers*, 2002, pp. 54–57.

[14] D. Oh and X. Yuan, *High-Speed Signaling*. Englewood Cliffs, NJ, USA: Prentice-Hall, 2012.

[15] F. Lambrecht, C.-C. Huang, and M. Fox, "Technique for determining performance characteristics of electronic systems," U.S. Patent 6775809, Mar. 14, 2002.

[16] J. Park et al., "A novel stochastic model-based eye-diagram prediction method for 8B/10B and TMDS-encoded high-speed channels," *IEEE Trans. Electromagn. Compat.*, vol. 60, no. 5, pp. 1510–1519, Oct. 2018, doi: 10.1109/TEMC.2017.2766295.

[17] J. Park et al., "A novel eye-diagram prediction method for pulse amplitude modulation with N-level (PAM-N) on stacked through-silicon vias," *IEEE Trans. Electromagn. Compat.*, vol. 61, no. 4, pp. 1198–1206, Aug. 2019.

[18] J. Park et al., "Polynomial model-based eye diagram prediction methods for LFSR-based bit streams in PRBS test and scrambling," *IEEE Trans. Electromagn. Compat.*, vol. 61, no. 6, pp. 1867–1875, Dec. 2019, doi: 10.1109/TEMC.2019.2900055.

[19] J. Park and J. Kim, "Generator polynomial model-based eye diagram prediction method for Bose-Chaudhuri-Hocquenghem (BCH) code and Reed-Solomon (RS) code," *IEEE Trans. Electromagn. Compat.*, vol. 62, no. 1, pp. 240–248, Feb. 2020, doi: 10.1109/TEMC.2018.2881146.

[20] Y. Kim, J. Park, J. Kim, and Y.-I. Hayashi, "Statistical eye-diagram prediction method considering power/ground noise induced by simultaneous switching output (SSO) buffers," *IEEE Trans. Electromagn. Compat.*, vol. 62, no. 6, pp. 2547–2557, Dec. 2020, doi: 10.1109/TEMC.2020.2975202.

Junyong Park (Member, IEEE) received the B.S. degree in electronic and electrical engineering from Sungkyunkwan University, Suwon, South Korea, in 2014, the M.S. and Ph.D. degrees in electrical engineering from the Korea Advanced Institute of Science and Technology (KAIST), Daejeon, South Korea, in 2016 and 2019, respectively.

He was a Senior Engineer with DRAM design, SK Hynix, Icheon, South Korea, from 2019 to 2023. In March 2023, he was with the Missouri University of Science and Technology (formerly University of Missouri-Rolla), Rolla, MO, USA, and is currently a Postdoctoral Fellow with the Missouri S&T EMC Laboratory. His current research interests include statistical signal/power integrity for high-speed systems, next-generation packages, and IBIS-AMI.

Manho Lee (Member, IEEE) received the B.S., M.S., and Ph.D. degrees in electrical engineering from the Terabyte Interconnect and Package Laboratory, South Korea Advanced Institute of Science and Technology, Daejeon, South Korea, in 2010, 2012, and 2017, respectively.

He is currently a Postdoctoral Researcher with the Terabyte Interconnect and Package Laboratory, Daejeon, South Korea. His current research interests include the statistical eye diagram estimation of various channels in SERDES and signal/power integrity of through-silicon-via-based 2.5-D/3-D ICs

Shinyoung Park (Member, IEEE) received the B.S., M.S., and Ph.D. degrees in electrical engineering from the Korea Advanced Institute of Science and Technology, Daejeon, South Korea, in 2015, 2017, and 2021, respectively.

She is currently a Senior Member of the Technical Staff with Signal Integrity, Rambus, San Jose, CA, USA, where she is responsible for package design and system-level signal and power integrity analysis for double data rate registering clock driver and data buffer development.

Jonghoon Kim (Senior Member, IEEE) received the Ph.D. degree in electrical engineering from the Korea Advanced Institute of Science and Technology (KAIST), Daejeon, South Korea, in 2003.

His doctoral dissertation was focused on the reduction of electromagnetic interference (EMI) from high-speed digital systems. After receiving the Ph.D. degree, he was with the Memory Division, Samsung Electronics, Suwon, South Korea, in 2003. Since joining Samsung Electronics, his experience has been in the standardization for DDR3/DDR4 memory and the simultaneous switching noise simulation considering real DRAM and real printed circuit board design data. He moved to the Department of Electrical Engineering, KAIST, in 2010, where he is currently a Research Professor. His current research interests include the analysis and design of wireless power transfer for electric vehicles as well as signal integrity, power integrity, and EMI of high-speed digital systems.

Joungho Kim (Fellow, IEEE) received the B.S. and M.S. degrees from Seoul National University, Seoul, South Korea, in 1984 and 1986, respectively, and the Ph.D. degree from the University of Michigan at Ann Arbor, Ann Arbor, MI, USA, in 1993, all in electrical engineering.

He was with the Memory Division, Samsung Electronics, Suwon, South Korea, in 1994, where he was involved in gigabit-scale DRAM design. In 1996, he was with the Korea Advanced Institute of Science and Technology (KAIST), Daejeon, South Korea. He is currently a Professor with the Department of Electrical Engineering, KAIST. He is also the Director of the three-dimensional (3-D) Integrated Circuit (IC) Research Center supported by SK Hynix Inc., Icheon, South Korea, and the Smart Automotive Electronics Research Center supported by KET Inc., Incheon. He has authored a book titled *Electrical Design of Through-Silicon-Via* (Springer, New York, NY, USA, 2014). In particular, his major research interests include chip package printed circuit board codesign and cosimulation for signal integrity, power integrity, ground integrity, and radiated emission in 3-D-IC, through-silicon via, and interposer.

DongHyun (Bill) Kim (Member, IEEE) received the B.S., M.S., and Ph.D. degrees in electrical engineering from Korea Advanced Institute of Science and Technology, Daejeon, South Korea, in 2012, 2014, and 2018, respectively.

In 2018, he was with the Missouri University of Science and Technology (formerly University of Missouri-Rolla), Rolla, MO, USA, and is currently an Assistant Professor with the Missouri S&T EMC Laboratory, Rolla, MO, USA. His current research interests include nanometer-scale devices, through-silicon via technology, dielectric material characterization and signal integrity, power integrity, temperature integrity, electromagnetic compatibility, and electrostatic discharge in 2.5D/3D IC (Integrated Circuit) systems.

Dr. Kim is a recipient of IEEE Region 5 Outstanding Young Professional (formerly GOLD) Award, IEEE St. Louis Section Outstanding Young Engineer Award, IEEE APEMC Outstanding Young Scientist Award and DesignCon Best Paper Award. He is a corecipient of DesignCon Early Career Best Paper Awards and IEEE EMC Symposium Best Paper Awards. He is currently the vice-chair of IEEE EMC Society TC-10 (Signal Integrity and Power Integrity) and the Chair of IEEE St. Louis Section.